

## A theoretical approach of the propagation through geometrical constraints in cardiac tissue

Sabir Jacquir, Stéphane Binczak, Jean-Marie Bilbault, Pierre Athias

► **To cite this version:**

Sabir Jacquir, Stéphane Binczak, Jean-Marie Bilbault, Pierre Athias. A theoretical approach of the propagation through geometrical constraints in cardiac tissue. International journal of bifurcation and chaos in applied sciences and engineering , World Scientific Publishing, 2007, 17 (12), pp.4417-4424. hal-00584227

**HAL Id: hal-00584227**

**<https://hal-univ-bourgogne.archives-ouvertes.fr/hal-00584227>**

Submitted on 7 Apr 2011

**HAL** is a multi-disciplinary open access archive for the deposit and dissemination of scientific research documents, whether they are published or not. The documents may come from teaching and research institutions in France or abroad, or from public or private research centers.

L'archive ouverte pluridisciplinaire **HAL**, est destinée au dépôt et à la diffusion de documents scientifiques de niveau recherche, publiés ou non, émanant des établissements d'enseignement et de recherche français ou étrangers, des laboratoires publics ou privés.

# A theoretical approach of the propagation through geometrical constraints in cardiac tissue

S. Jacquir<sup>1</sup>, S. Binczak<sup>1</sup>, P. Athias<sup>2</sup>, J.M Bilbault<sup>\*,1</sup>

*Laboratoire LE2I UMR CNRS 5158, Aile des Sciences de l'Ingénieur, Université de Bourgogne, BP 47870, 21078 Dijon Cedex, France<sup>1</sup>*

*Institut de Recherche Cardiovasculaire, CHU Le Bocage, Dijon, France<sup>2</sup>*

bilbault@u-bourgogne.fr<sup>\*</sup>

---

## Abstract

The behaviour of impulse propagation in the presence of non-excitabile scars and boundaries is a complex phenomenon and induces pathological consequences in cardiac tissue. In this article, a geometrical configuration is considered so that cardiac waves propagate through a thin strand, which is connected to a large mass of cells. At this interface, waves can slow down or even be blocked depending on the width of the strand. We present an analytical approach leading to determine the blockade condition, by introducing planar travelling wavefront and circular stationary wave. Eventually, the influence of the tissue geometry is examined on the impulse propagation velocity.

*Key words:* Travelling wavefront; Circular stationary wave; Blockade phenomenon; Cardiac tissue.

---

## 1 Introduction

Reentry is the major mechanism of life-threatening ventricular arrhythmias associated with myocardial infarction scars [Myerburg et al., 1997]. In abnormal conditions, electrical cardiac wavefront may be stopped by, for instance, electrically non-excitable scar or functional block, which may induce a reentry circuit in pathological endocardial tissue. Nevertheless, normal geometrical features may also imply variations of the conduction properties, as accessory atrioventricular pathways, consisting of narrow strands of myocytes coursing from atrium to ventricle [Saffitz, 2005]. Therefore, the architecture of the cellular network forming the myocardium [Rohr et al., 1997; Wang & Rudy, 2000] and the geometry of excitation wavefront [Fast & Kleber, 1997, 1995a,b] are important to characterize the impulse propagation. Mathematical models [Kleber & Rudy, 2004; Noble, 1962] and nonlinear dynamics are widely used to study the impulse (action potential) propagation in cardiac cells [Murray, 1989; Keener & Sneyd, 1998; Scott, 1999]. Among them, one of the major model is described by the FitzHugh-Nagumo (FHN) equation [FitzHugh, 1961; Nagumo et al., 1962], which allows analytical approaches. The goal of this paper is to study the propagation condition in a system composed of a thin strand of myocytes connected to a large mass of myocytes. This geometry is modeled using a modified version of the FHN 2D equation. We show that, at the interface of the two parts of the system, the shape of the waves goes through a geometrical modification, which can lead to a decrease of the velocity up to a blockade phenomenon. Eventually, we determine the

---

optimal width of the strand which minimizes the time delay at the interface.

## 2 Analytical determination of the propagation condition

We consider a thin sheet of myocardium such as a two-dimensional model is used to describe the impulse propagation. The medium is assumed to be isotropic and its schematic design is sketched in Fig. 1. In the bounded domain  $\Omega$ , domain (1) is the corridor of width  $l_1$ , domain (2) is the corridor of width  $l_2$  with  $l_2 > l_1$  and the corresponding equations modelling this system are:

$$\begin{cases} \frac{\partial V}{\partial t} = D\Delta V - f(V) - W \\ \frac{\partial W}{\partial t} = \varepsilon(V - \gamma W) , \end{cases} \quad (1)$$

where  $D$  is the diffusion parameter,  $t$  is the time,  $\Delta$  is the continuous Laplacian operator,  $V$  is the transmembrane voltage.  $W$  is the recovery variable, which indicates the capacity of the medium to revert to its resting state after the propagation of impulses due to potassium current and the nonlinear function  $f(V)$  represents the behaviour of the sodium current (it also includes a leak potassium current [Scott, 2002]). Usually,  $f(V)$  is a cubic polynomial function, but a common simplification is to approximate this function by a piecewise linear expression [Fath, 1998]. Furthermore, characterizing the velocity of the action potential can be performed by determining the velocity of the leading edge of this wave, which is given by the condition  $W(t) = 0 \forall t$ . The system (1) becomes

$$\frac{\partial V}{\partial t} = D\Delta V - [V - H(V - \alpha)], \quad (2)$$

where  $\alpha$  is a threshold between the passive and the active role of the sodium conductance ( $0 < \alpha < 1/2$ ) and  $H$  is the Heaviside step function. This system is completed by the Neumann boundary conditions, so that

$$\left(\frac{\partial V}{\partial n}\right)_{\delta\Omega} = 0, \quad (3)$$

where  $\left(\frac{\partial}{\partial n}\right)_{\delta\Omega}$  denotes the outer normal derivative at the boundary  $\delta\Omega$  of the bounded domain  $\Omega$ . To investigate a propagation at the interface, we initiate a wavefront in domain (1). Due to the width of the strand, we assume this wave to be planar and propagating towards domain (2). The symmetry induced by this choice of configuration leads to reduce the system in domain (1) to a continuous one-dimensional medium so that it can be described by the following bistable equation,

$$\frac{\partial V}{\partial t} = D \frac{\partial^2 V}{\partial x^2} - [V - H(V - \alpha)]. \quad (4)$$

Introducing the travelling frame coordinate  $\xi = x - ct$ , where  $c$  is the front velocity and  $x$  is the spatial parameter representing the longitudinal axis of the strand, Eq. (4) can be written so that

$$D \frac{\partial^2 V}{\partial \xi^2} + c \frac{\partial V}{\partial \xi} - [V - H(V - \alpha)] = 0, \quad (5)$$

which yields, due to  $C^0$  continuity, the propagating solution in domain (1):

$$\begin{cases} V(\xi) = \alpha e^{\lambda_{2,1}\xi}, & \text{if } V < \alpha \\ V(\xi) = (\alpha - 1)e^{\lambda_{1,2}\xi} + 1, & \text{if } V \geq \alpha, \end{cases} \quad (6)$$

where  $\lambda_{1,2} = -\frac{c}{2D} \pm \frac{1}{2}\sqrt{\left(\frac{c}{D}\right)^2 + \frac{4}{D}}$ .

Note that in [Zemskov et al., 2000], the stability of this kind of solution in an infinite medium has been analyzed. Note also that this solution has been observed and confirmed by numerical simulations.

When this wave reaches the interface, a symmetry breaking occurs, depending on the width  $l_1$  (resp.  $l_2$ ) of the domain (1) (resp. domain (2)) leading to different scenarios:

- if  $l_1 \leq l_c \ll l_2$ , the incoming wave is pinned at the interface (see Fig (8)), where  $l_c$  is a critical width to be determined,
- if  $l_2 > l_1 > l_c$ , the wave is transformed in either circular ( $l_1$  small) or elliptic one ( $l_1$  large) (see Fig (9)),
- if  $l_1 = l_2$ , we observe a planar propagation in domain (2), according to Eq. (6).

In the blockade situation, numerical simulations show that the shape of the stationary wave is circular. Therefore, it corresponds to the existence of a circular stationary solution in domain (2), precluding the possibility of a propagating front.

In order to determine the critical value  $l_c$ , we need to express the stationary solution in the case of a circular wave. Because of this circular symmetry, we look for a time independent solution  $V(r)$  with  $r$  radial coordinate, leading to express Eq. (2), so that

$$D\left(\frac{\partial^2 V}{\partial r^2} + \frac{1}{r} \frac{\partial V}{\partial r}\right) = V - H(V - \alpha). \quad (7)$$

Introducing  $\rho = r\sqrt{\frac{1}{D}}$ , Eq. (7) becomes

$$\left(\frac{\partial^2 V}{\partial \rho^2} + \frac{1}{\rho} \frac{\partial V}{\partial \rho}\right) = V - H(V - \alpha), \quad (8)$$

leading to two versions of the modified Bessel equation:

- if  $V < \alpha$ , Eq. (8) becomes  $\frac{\partial^2 V}{\partial \rho^2} + \frac{1}{\rho} \frac{\partial V}{\partial \rho} - V = 0$  and the stationary solution is

$$V(\rho) = A_1 I_0(\rho) + B_1 K_0(\rho), \quad (9)$$

where  $I_0$  and  $K_0$  represent the modified Bessel functions of the first and second kind respectively.

- if  $V \geq \alpha$ , Eq. (8) becomes  $\frac{\partial^2 V}{\partial \rho^2} + \frac{1}{\rho} \frac{\partial V}{\partial \rho} - V + 1 = 0$  and the stationary solution is

$$V(\rho) = 1 + A_2 I_0(\rho) + B_2 K_0(\rho). \quad (10)$$

We impose the following conditions leading to find the constants  $A_1$ ,  $B_1$ ,  $A_2$  and  $B_2$ :

- $V(r \rightarrow \infty) = 0$  leading to  $A_1 = 0$ .
- $V(r = 0) = V_0 > \alpha$  leading to  $B_2 = 0$ .

Eventually, due to  $C^0$  continuity at  $r = r_a$  where  $V(r_a) = \alpha$ , we get for the stationary wave solution

$$\begin{cases} V(r) = \frac{\alpha K_0\left(\frac{r}{\sqrt{D}}\right)}{K_0\left(\frac{r_a}{\sqrt{D}}\right)}, & \text{if } r \geq r_a \\ V(r) = 1 + (\alpha - 1) \frac{I_0\left(\frac{r}{\sqrt{D}}\right)}{I_0\left(\frac{r_a}{\sqrt{D}}\right)}, & \text{if } r < r_a. \end{cases} \quad (11)$$

Moreover,  $r_a$  is determined by:

$$r_a = \sqrt{D} I_0^{-1} \left( \frac{\alpha - 1}{V_0 - 1} \right). \quad (12)$$

In Eq. 11,  $V_0$  is the maximal amplitude of an initial condition corresponding to  $r = 0$  and is expressed by

$$V_0 = 1 + \frac{\alpha - 1}{I_0(\sqrt{\frac{1}{D}} r_a)} \quad (13)$$

The value of  $V_0$  only depends on the nonlinear threshold  $\alpha$  and it is not influenced by the diffusion properties of the tissue (see Fig 2).

An illustration of a circular stationary wave is presented in Fig. 3. The stationary solution given by Eq. (11) allows the determination of the critical width  $l_c$ . Indeed, the blockade situation corresponds to the case where an incoming planar propagating wave in domain (1) gives birth to the circular stationary wave in domain (2). In this configuration, and due to the boundary conditions, only the half plane solution of Eq. (11) is taken into account.

The numerical simulations (see Figs (8) and (9)) show that at first approximation, it is necessary that at least a half-disc of radius  $r_c$  is under excited conditions, i.e. with  $V > \alpha$ . Thus, for calculating a minimal area generating a propagation,  $r_a$  is assumed to be equal to  $r_c$ .

In order to determine  $r_c$ , we use an analogy of Eq. (7) with the Poisson equation used in the field of electrostatic phenomena. The theorem of the divergence is given by

$$\int_{surf} \overrightarrow{grad} V \cdot \overrightarrow{dS} = \int_{vol} \Delta V \cdot d\tau \quad (14)$$



where  $surf$  is the closed surface directed towards outside and  $vol$  is the interior volume.

In our case, the study is restricted to a thin sheet of cells, i.e a bidimensional medium. Therefore, the theorem (14) becomes

$$\int_{lig} \overrightarrow{grad} V \cdot \overrightarrow{dM} = \int \int_{surf} \Delta V \cdot dS, \quad (15)$$

where  $lig$  is the closed line directed towards outside and  $surf$  is the interior surface.

We calculate the two terms of Eq. (15).  $J_1$  is the integral corresponding to the closed line and  $J_2$  is the integral of the interior surface.

Referring to Fig. (4),  $J_1 = \phi_1 + \phi_2$  where  $\phi_1$  and  $\phi_2$  are flows.

Thus, the flow coming from the domain (1) is given by

$$\phi_1 = -2r_c \frac{(V_i - 1)}{\sqrt{D}}, \quad (16)$$

with  $V_i$  corresponds to the value of the wave to the interface of the two domains given by Eq (13). In addition, the outgoing flow of the half-disc, calculated from Eq. (11), is given by

$$\phi_2 = -\pi\alpha \frac{r_c}{\sqrt{D}} \frac{K_1\left(\frac{r_c}{\sqrt{D}}\right)}{K_0\left(\frac{r_c}{\sqrt{D}}\right)}. \quad (17)$$

Then  $J_2 = \int \int_{surf} \Delta V \cdot dS = \int \int \frac{f(V)}{D} dS = \int_{r=0}^c \frac{V-1}{D} \pi r dr$ , as when  $V > \alpha$ ,  
 $f(V) = V - 1$ , with  $V = 1 + (\alpha - 1) \frac{I_0\left(\frac{r}{\sqrt{D}}\right)}{I_0\left(\frac{r_c}{\sqrt{D}}\right)}$ .

The integral  $J_2$  is thus expressed by

$$J_2 = \int_0^{r_c} \frac{(\alpha - 1) I_0\left(\frac{r}{\sqrt{D}}\right)}{D I_0\left(\frac{r_c}{\sqrt{D}}\right)} \pi r dr. \quad (18)$$

Setting  $z = \frac{r}{\sqrt{D}}$  and using the fact that  $I_0(Z)$  is very appreciably constant and equal to 1 as long as  $|z| \ll 1$ ,  $J_2$  can be evaluated and expressed by:

$$J_2 = \frac{\pi r_c^2 (\alpha - 1)}{2D I_0\left(\frac{r_c}{\sqrt{D}}\right)}. \quad (19)$$

Thus the critical width  $l_c$  of the domain (1), corresponding to the blockade of the wave, is obtained implicitly from  $r_c$ , knowing that  $l_c = 2r_c$ . The value of  $r_c$  is given by  $J_1 - J_2 = 0$ :

$$\left(\frac{4}{\pi} + \frac{r_c}{\sqrt{D}}\right) \frac{(1 - \alpha)}{I_0\left(\frac{r_c}{\sqrt{D}}\right)} - 2\alpha \frac{K_1\left(\frac{r_c}{\sqrt{D}}\right)}{K_0\left(\frac{r_c}{\sqrt{D}}\right)} = 0. \quad (20)$$

A comparison between this theoretical prediction and numerical simulations shows a good match between them as illustrated in Fig. 5 (based on a finite difference scheme using a 4<sup>th</sup> order Runge-Kutta on a 100 \* 100 adaptative mesh). This good correlation is in fact a justification a posteriori of the assumption that a half disc of ray  $r_c = \frac{l_c}{2}$  must have its cells in excited state (i.e.  $V > \alpha$ ) so that the propagation initiated in the corridor can continue in the wide second medium. Our study gives in fact a little severe condition on  $l_c$  as one can see it on the figure (5). It would be interesting of to continue this study by considering a propagation going from a broad domain to a narrow domain (for example in one kind of bottleneck).

In addition to the blockade phenomenon confirmed numerically when  $l_1 \leq l_c$ , the numerical simulations indicate that the wave propagation in the domain (2) induced a delay because of the transformation of the planar wave in a

curved wavefront. In fact, this delay is necessary so that the cells reach their excitation threshold, such as is observed in experiments [Saffitz, 2005]. In the following part, numerical simulations showing the relationship between the velocity of the wave, the intrinsic parameters of the model and the geometrical characteristics of the cardiac tissue are presented.

### 3 Wavefront velocities in the medium

Besides the numerical confirmation of the blockade phenomenon when  $l_1 \leq l_c$ , numerical simulations indicate that the emergence of propagating wave in domain (2) induces a time delay due to the transformation of the planar travelling wave to a non-zero curvature wavefront. Actually, this delay is required so that cells reach the threshold excitation, as observed experimentally [Saffitz, 2005]. In this section, we present a numerical study showing the relationship between velocity, intrinsic parameters of the model and geometrical features. The basic morphological features of the transition region between a domain (1) and a domain (2) are depicted on Fig. 6, where  $l$  is the width of the domain (1),  $v_c$  is the wavefront velocity between two positions along the longitudinal axis in the domain (1),  $v_o$  is the wavefront velocity between two positions along the longitudinal axis in the domain (2) and  $v_t$  is the wavefront velocity between one position in the domain (1) and a second position along the longitudinal axis in the domain (2). As previously described, we initiate a planar wavefront in the corridor travelling towards the large area. Figure 7 shows the different velocities of the wavefront when  $\alpha = 0.4$  and  $D = 0.5$ , in function of  $l$  (expressed in cell number). The results indicate that the velocity of the circular wave in domain (2) depends on the width  $l$  of the strand, which changes the

curvature of the transformed wave, as suggested in [Kogan et al., 1992]. The numerical results illustrate the fact that there exists a critical value  $l_c$  of  $l$  below which the wavefront fails to propagate through the subdomains interface, as shown in Fig. 8. When  $l$  is large enough, velocities are equal and the wavefront is no more influenced by the interface. Between these two cases, the symmetry breaking implies a time delay corresponding to the geometrical transformation of the wave from a planar to a non planar wavefront (see Fig. 9 for instance, where a circular wave appears just after the transition region). Let  $t_a$  be the necessary normalized time needed to the wavefront to cross the interface so, that

$$t_a = \frac{\frac{d_t}{v_t} - \frac{d_o}{v_o} - \frac{d_c}{v_c}}{\frac{d_o}{v_o} + \frac{d_c}{v_c}} \quad (21)$$

with  $d_i$ , the distance between the different parts of the medium for which the velocity  $v_i$  ( $i=\{t,o,c\}$ ) is measured. Figure 10 shows that this overall delay can be either positive or negative depending on the value of  $l$ . Note that delays may imply reentrant arrhythmias due to a lack of synchronicity between wavefront coming from different pathways. Our results indicate that, besides the case of large corridors, there exists an optimum width  $l_{opt}$  around which overall delays are negligible (see Fig. 10). Therefore, there is a possible relationship between length and width of corridors preventing dramatic changes of cardiac activity.

#### 4 Discussion and conclusions

In this study, an analytical solution of travelling front in the case of the planar propagation has been determined. The criterion for the initiation of the cir-

cular waves has been investigated, based on the existence of stationary waves. We showed that the existence of the stationary wave prevents the propagation. Again, this breakdown depends not only on the nonlinearity threshold and on the diffusion coefficient but also on the geometrical morphology of the cardiac syncytium and on the form of the excitation wavefront. However, our results concerning the condition of propagation are valid in the case of a very thin strand of cells (domain 1). To generalize and to refine our approach, it would be necessary to use the spheroidal functions using the elliptic coordinates. There exists specific geometric configuration of two-dimensional narrow pathways, which allow unidirectional conduction blocks and reentry even when membrane properties and intercollated resistance are uniform [Kogan et al., 1992]. We suggest that this work could be applied to avoid the reentry phenomena. In other words, our results could modify the strategies used during arrhythmia ablation procedures. Indeed, precise radiofrequency applications inside scar tissues could improve conduction velocity in other areas and prevent reentries [Chillou et al, 2002]. It would correspond to fix the optimized width so that the delay becomes negligible, which would assure synchronicity between waves coming from different pathways.

## References

- Chillou, C., Lacroix, D., Klug, D., Magnien-Poull, I., Marquie, C., Messier, M., Andronache, M., Kouakam, C., Sadoul, N., Chen, J., Aliot, E. & Kacet, S. [2002] "Isthmus characteristics of reentrant ventricular tachycardia after myocardial infarction", *Circulation*. 105(6), 726-731.
- Fast, V.G. & Kleber, A.G. [1995] "Cardiac tissue geometry as a determinant of unidirectional conduction block: assessment of microscopic excitation spread by optical mapping in patterned cell cultures and in a computer model", *Cardiovascular Research*. 29, 697-707.
- Fast, V.G. & Kleber, A.G. [1995] "Block of impulse propagation at an abrupt tissue expansion: evaluation of the critical strand diameter in 2- and 3-dimensional computer models", *Cardiovascular Research*. 30, 449-459.
- Fast, V.G. & Kleber, A.G. [1997] "Role of wavefront curvature in propagation of cardiac impulse", *Cardiovascular Research*. 33, 258-271.
- Fath, G. [1998] "Propagation failure of traveling waves in a discrete bistable medium", *Physica D*. 116, 176-190.
- FitzHugh, R. [1961] "Impulses and physiological states in theoretical models of nerve membrane", *Biophys. J.* 1, 445-466.
- Keener, J.P. & Sneyd, J. [1998] "Mathematical Physiology", *IAM Springer-Verlag, Berlin*.
- Kleber, A.G. & Rudy, Y. [2004] "Basic mechanisms of cardiac impulse propagation and associated arrhythmias", *Am. Physiol. Rev.* 84, 431-488.
- Kogan, B.Y., Karplus, W.J., Billett, B.S. & Stevenson, W.G. [1992] "Excitation wave propagation within narrow pathways: Geometric configurations facilitating unidirectional block and reentry", *Physica D*. 59, 275-296.
- Murray, J.D. [1989] *Mathematical Biology*, (Springer-Verlag, Berlin).

- Myerburg, R.J., Interian, A., Mitrami, R.M., Kessler, K.M. & Castellanos, A. [1997] "Frequency of sudden cardiac death and profiles of risk", *Am. J. Cardiology*. 80, 10F-19F.
- Nagumo, J., Arimoto, S. & Yoshizawa, S. [1962] "An active impulse transmission line simulating nerve axon", *Proc. IRE*. 50, 2061-2070.
- Noble, D. [1962] "A modification of the Hodgkin-Huxley equation applicable to Purkinje fibre action and pacemaker potentials", *J. Physiol.* 160, 317-352.
- Rohr, S., Kucera, J.P. & Kleber, A.G. [1997] "Form and function: Impulse propagation in designer cultures of cardiomyocytes", *News Physiol. Sci.* 12.
- Saffitz, J.E. [2005] "The pathology of sudden cardiac death in patients with ischemic heart disease-arrhythmology for anatomic pathologists", *Cardiovascular Pathology*. 14, 195-203.
- Scott, A.C. [1999] *Nonlinear Science*, (Oxford University Press, NY).
- Scott, A.C. [2002] *Neuroscience*, (Springer, NY).
- Wang, Y. & Rudy, Y. [2000] "Action potential propagation in inhomogeneous cardiac tissue: Safety factor consideration and ionic mechanism", *Am. J. Physiol.* 278, H1019.
- Zemskov, E.P., Zykov, V.S., Kassner, K. & Müller, S.C. [2000] "Stability of travelling fronts in a piecewise-linear reaction-diffusion system", *Nonlinearity*. 13, 2063-2076.

## 5 Captions

Fig1: Schematic diagram of the geometry of the tissue.  $l_1$  (resp.  $l_2$ ) is the width of the domain (1) (resp. domain (2)). Arrow indicates direction of propagation.

Fig2: Initial condition  $V_0$  versus  $\alpha$  for all diffusion parameter  $D$ .

Fig3: Cross-section of the standing wave with  $D = 1$ ,  $\alpha = 0.2$ ,  $r_a = 0.8186$  leading to  $V_0 = 0.319$ .

Fig4: Diagram illustrating flows entering and outgoing of the half disc of ray  $r_c$ .

Fig5:  $l_c$  versus  $\alpha$  ( $D = 1$ ). Theoretical results (cf Eq.(??)) in continuous line (crosses), numerical results in dashed line (stars) with error bars  $\pm 0.05$ .

Fig6: Schematic diagram of the geometry of the tissue using during simulation.  $l$  is the width of the thin strand and  $d_i$  is the distance between the different parts of the medium for which the velocity  $v_i$  ( $i=\{t,o,c\}$ ) measured.

Fig7: Wavefront normalized velocity versus the width of the strand expressed in cell numbers with parameters  $D = 0.5$  and  $\alpha = 0.4$ .

Fig8: Simulation of the blockade phenomenon with parameters  $l < l_c$ ,  $D = 1$  and  $\alpha = 0.2$ .

Fig9: Simulation of the propagation phenomenon with parameters  $l > l_c$ ,  $D = 1$  and  $\alpha = 0.2$ .

Fig10: Time  $t_a$  versus the width of the strand expressed in cell numbers with parameters  $D = 0.5$  and  $\alpha = 0.4$ .



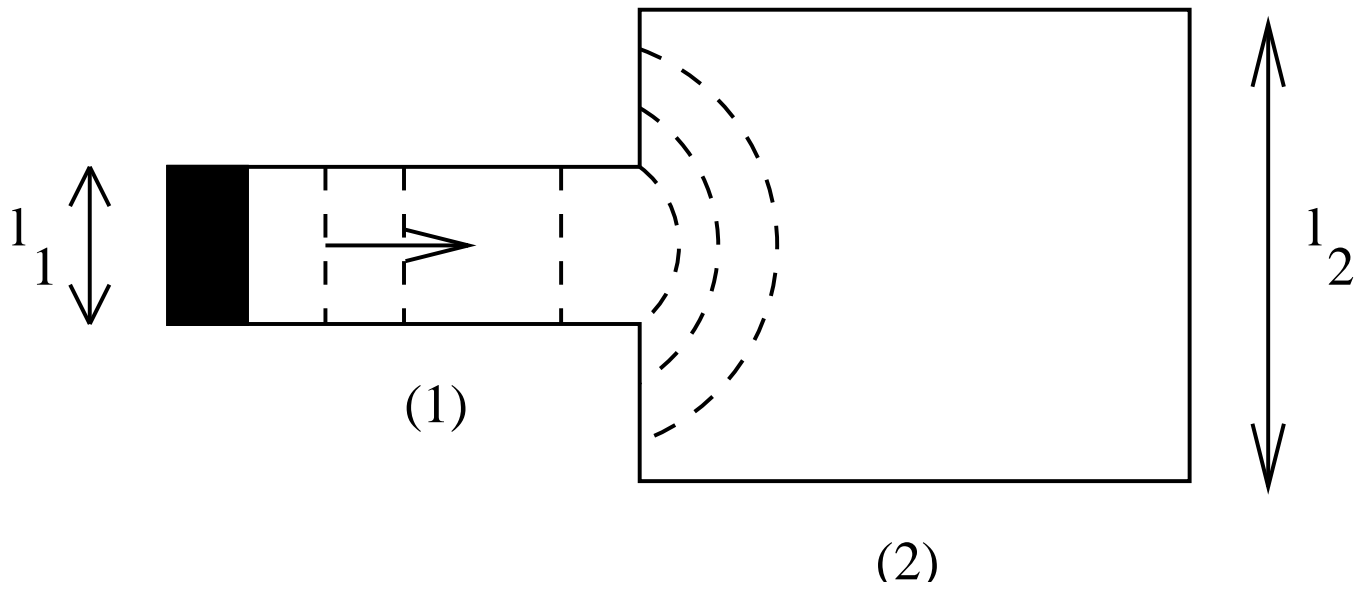


Fig. 1.

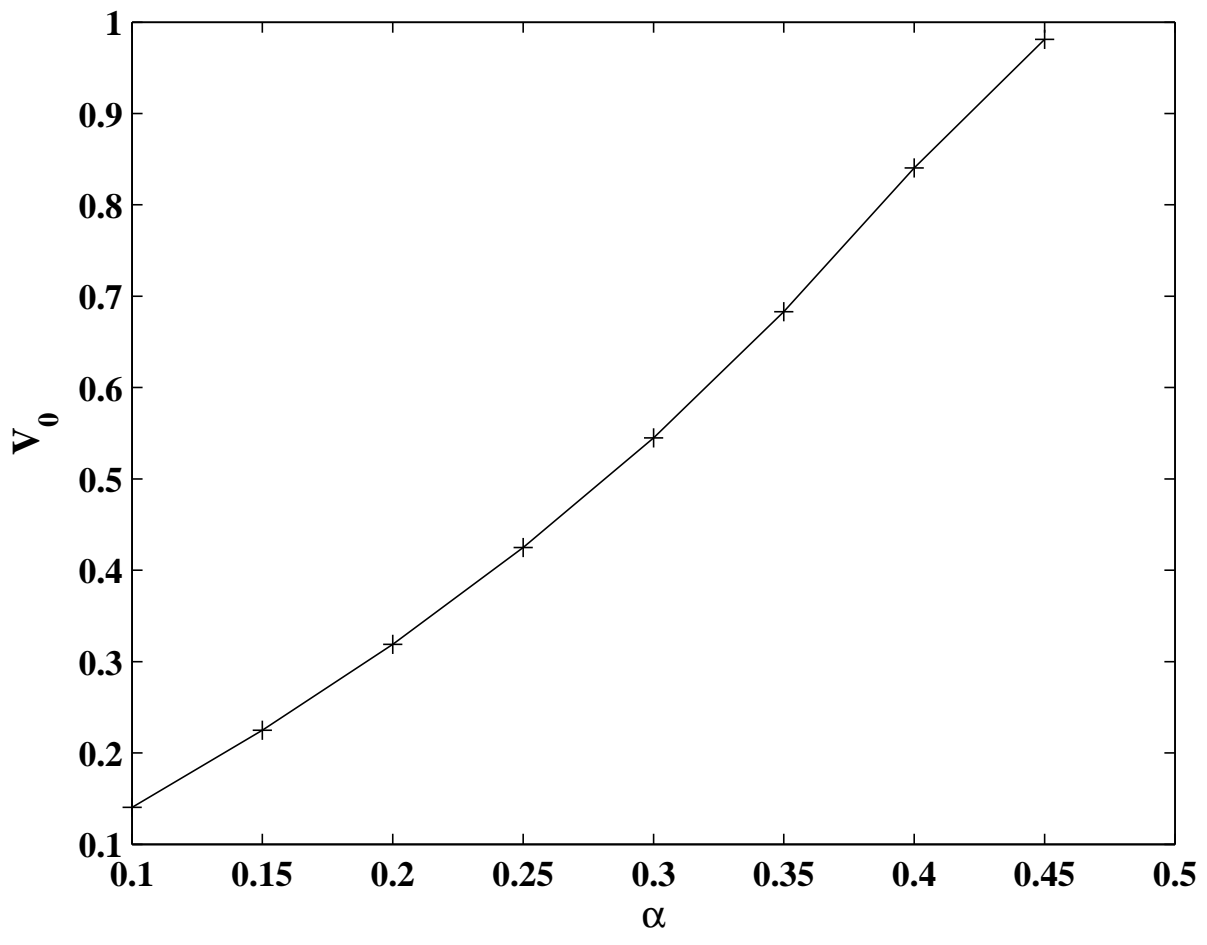


Fig. 2.

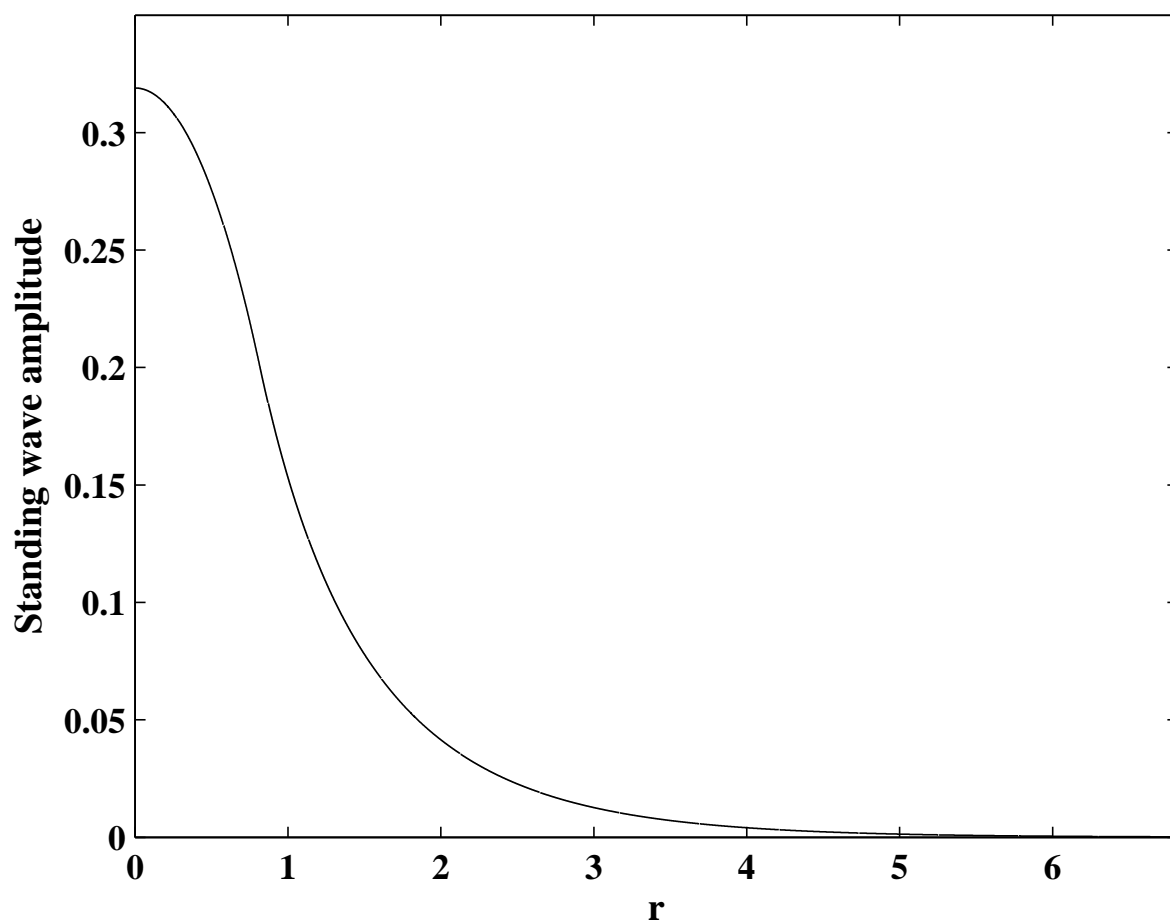


Fig. 3.

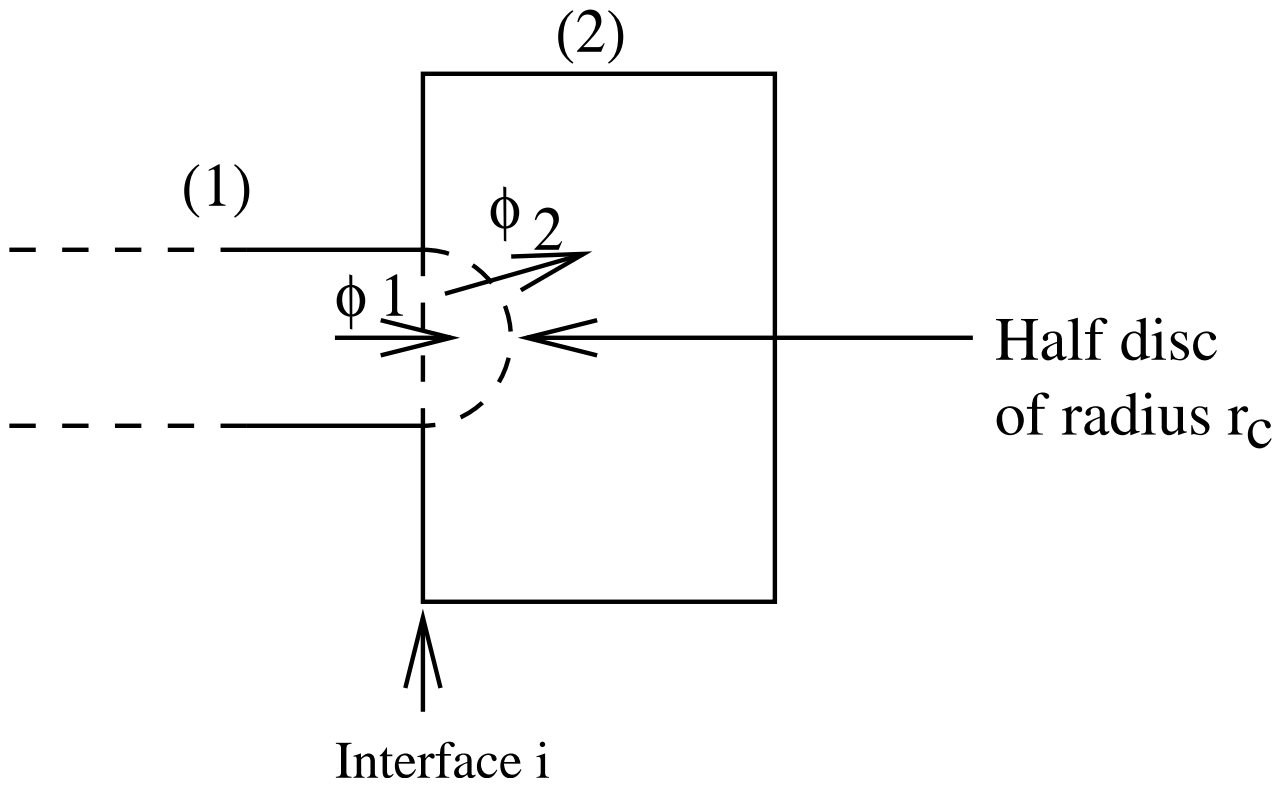


Fig. 4.

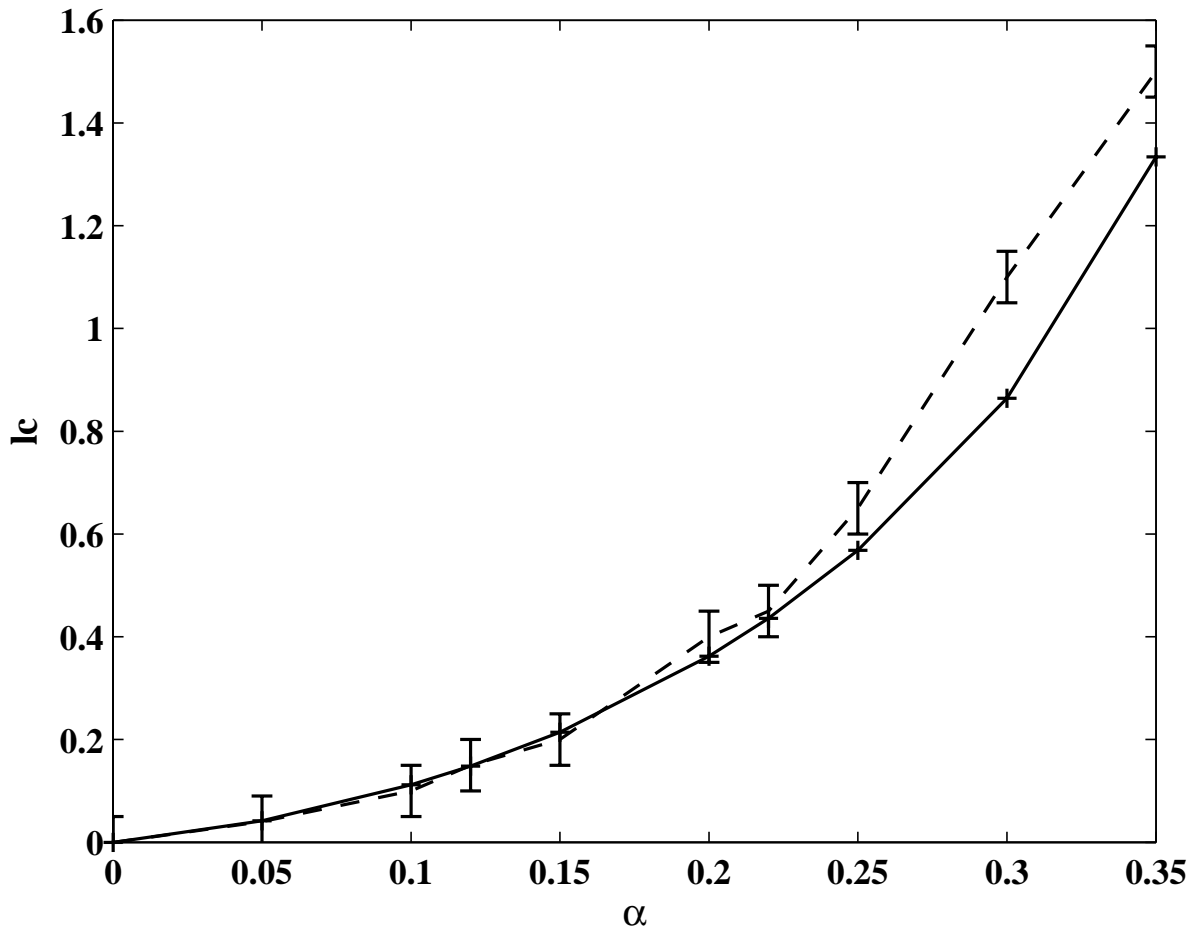


Fig. 5.

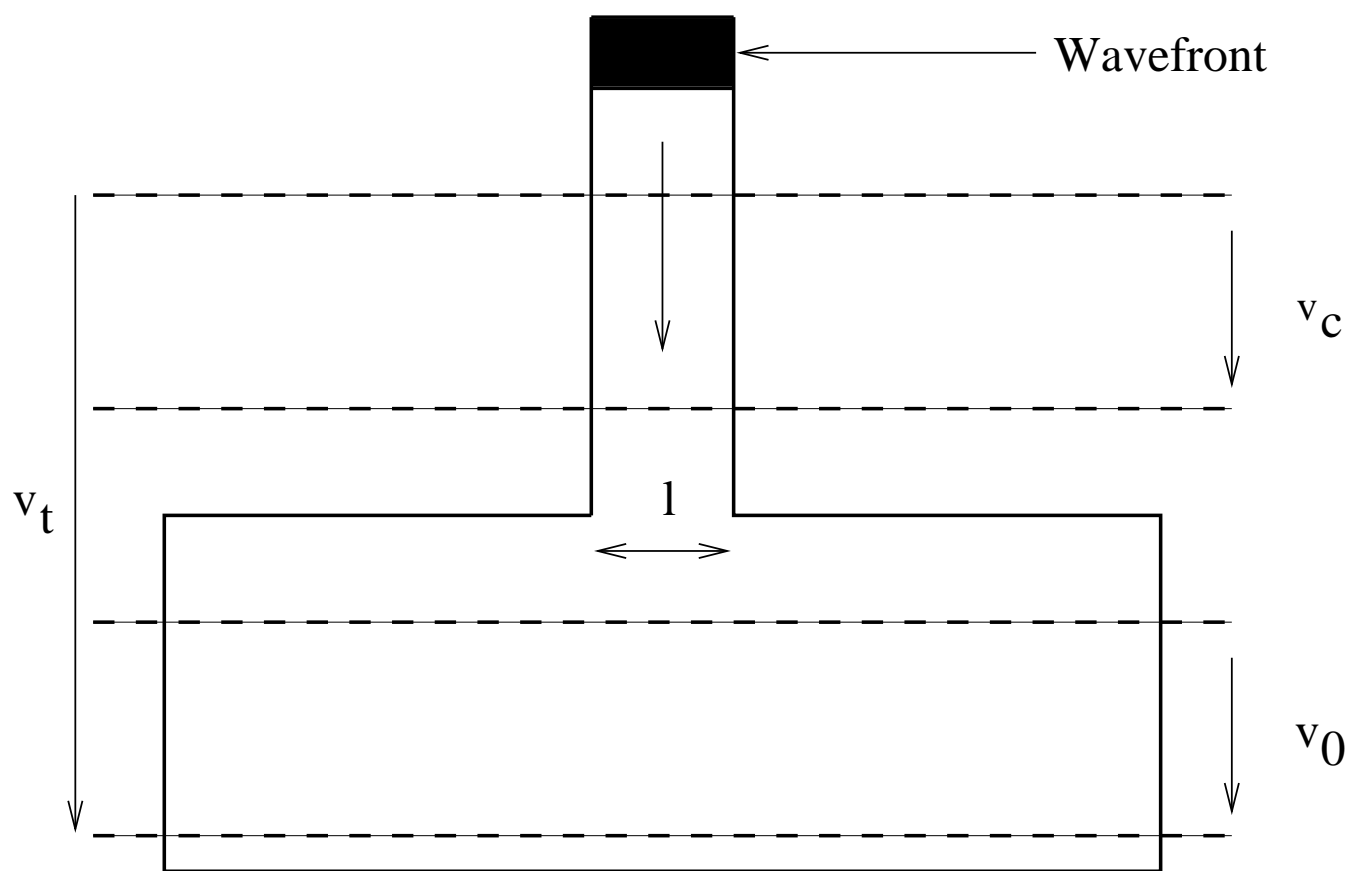


Fig. 6.

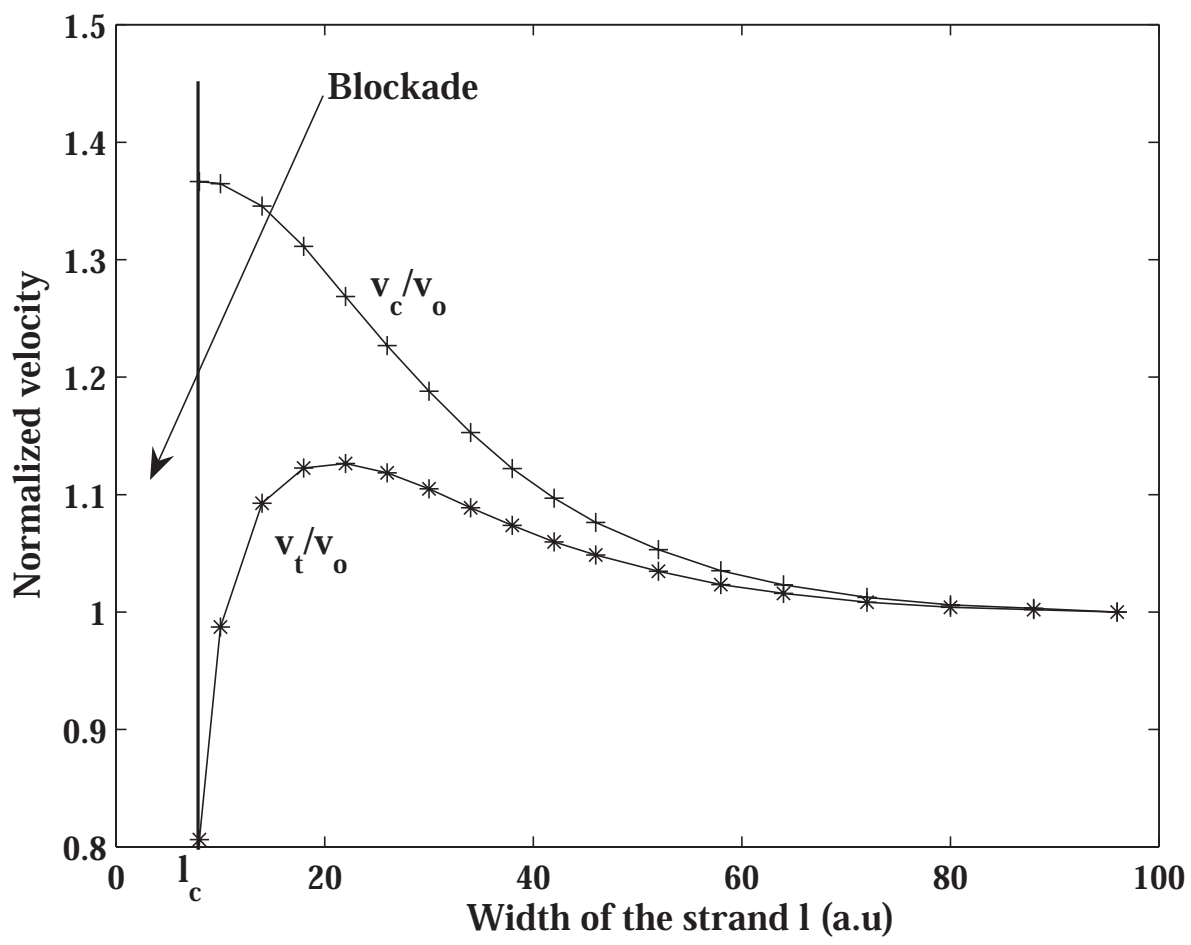


Fig. 7.

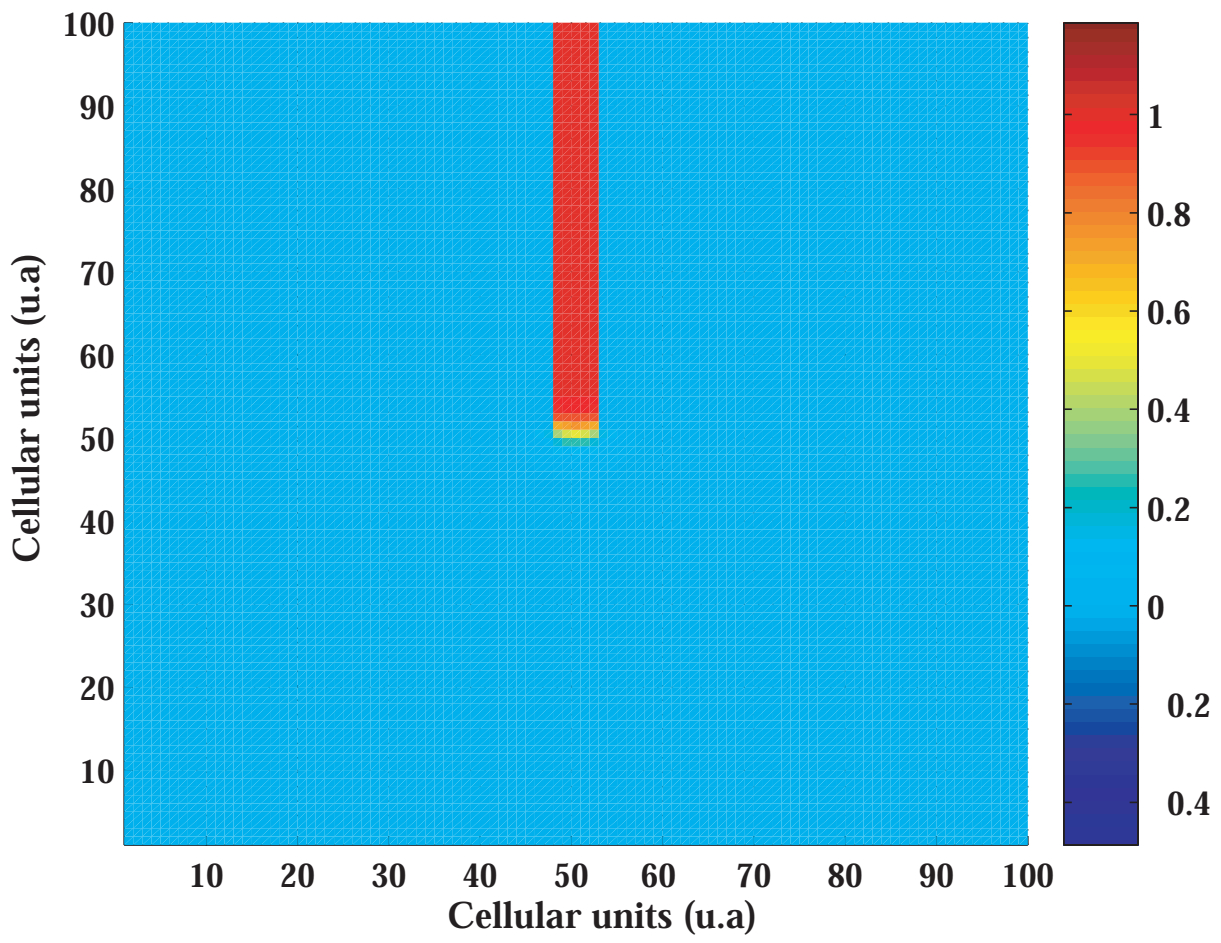


Fig. 8.



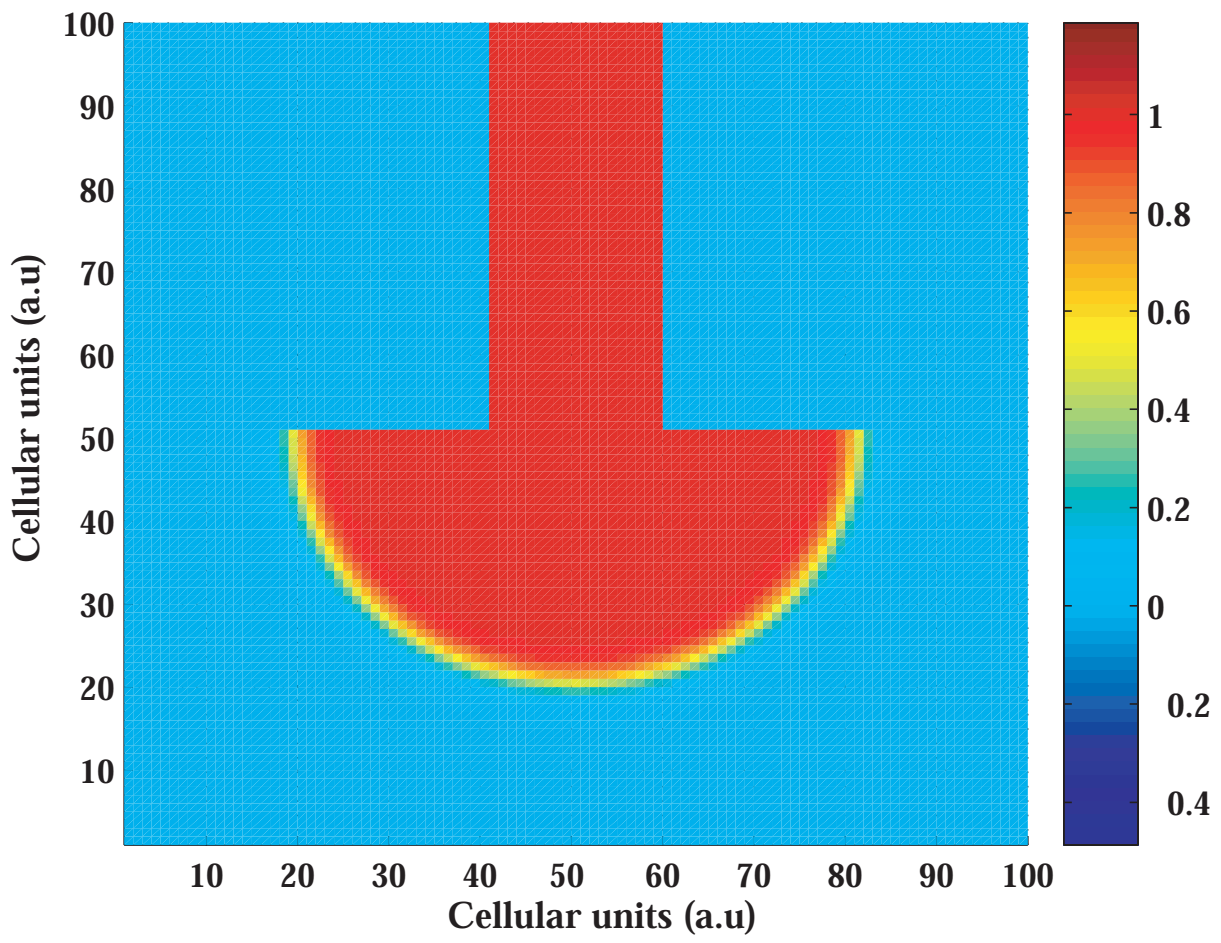


Fig. 9.

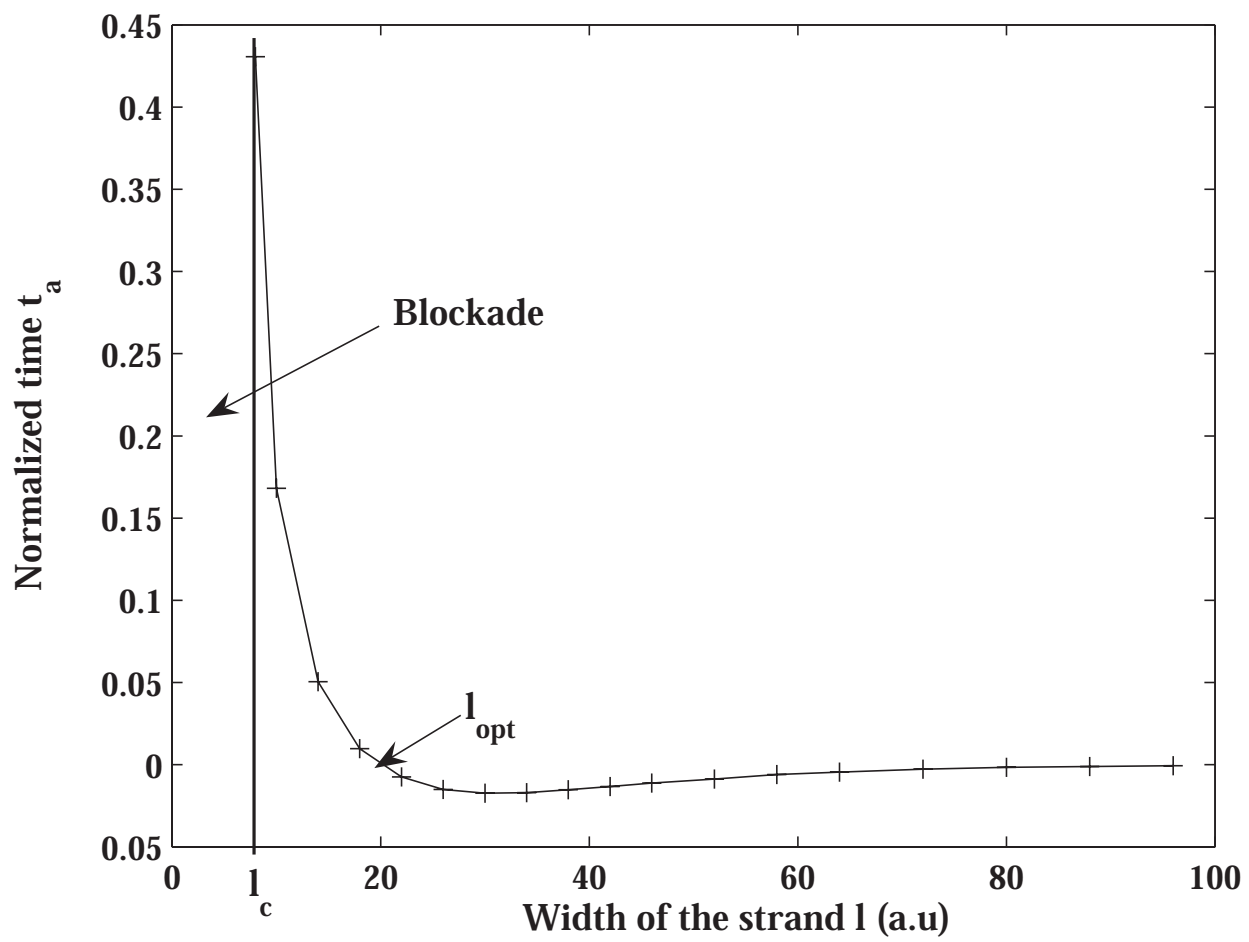


Fig. 10.